

SMASIS2018-8244

## VISCOELASTIC ESHELBY ANALYSIS OF CARDIOMYOCYTE CONTRACTION IN THE CELL-IN-GEL SYSTEM

Mohammad Kazemi-Lari \*; John Shaw, Alan Wineman  
University of Michigan, Ann Arbor, MI 48109

Rafael Shimkunas, Leighton Izu, Ye Chen-Izu  
University of California, Davis, CA 95616

### ABSTRACT

*We present a mathematical model to guide and interpret ongoing Cell-in-Gel experiments, where isolated cardiac myocytes are embedded in a constraining viscoelastic hydrogel, to study mechano-chemo-transduction mechanisms at the single cell level. A recently developed mathematical model, based on the elastic Eshelby inclusion problem, is here extended to account for viscoelasticity of the inclusion (cell) and the matrix (gel). The viscoelastic simulations indicate that the change in cell stiffness, as a result of the active up-regulation of the internal  $Ca^{2+}$  transients, has a strong influence on the contraction of the cell in response to the afterload. It is also found that increasing gel's crosslink density significantly alters the strain and stress fields inside the cell and yields to an increased time-lag in the response of the cell to the external stimulus.*

### INTRODUCTION

During each heartbeat, cardiac muscle cells experience mechanical stresses that continuously vary with physical activity, posture, emotion, and pathophysiological states. The healthy heart is an impressively “smart” structure, capable of upregulating its contraction and force in response to cardiac demands by the Frank Starling and Anrep mechano-chemo-transduction (MCT) mechanisms [1, 2]. Under pathological conditions, however, hemodynamic overload can trigger structural growth and remodeling that leads to arrhythmias, hypertrophy, dilation, or heart failure. A novel Cell-in-Gel system is being used to study MCT mechanisms at the single-cell level under normal and overload conditions in healthy and diseased states. The system con-

sists of isolated live cardiac myocytes that are embedded in a constraining hydrogel to mimic the *in vivo* mechanical environment during myocyte contraction. While cell contractions and strains can be measured directly, mechanical stresses must be inferred by analysis.

Here, we present a mathematical model to quantify all mechanical fields and to guide and interpret ongoing Cell-in-Gel experiments [3]. The proposed model is based on the classical Eshelby problem of an ellipsoidal inclusion embedded in an elastic matrix, which is extended here to account for the viscoelasticity of the inclusion (cell) and the matrix (gel). This provides more accurate calculations of time-dependent 3D stress and strain fields present during experiments.

Hydrogels of various cross-link densities are used in the Cell-In-Gel experiments to systematically vary the mechanical resistance to myocyte contraction. Hydrogels are viewed as hydrophilic three dimensional networks of polymer chains containing a large amount of water. These crosslinked polymer networks resemble elastic scaffolds surrounded by water molecules. Hydrogels are structurally similar to the extracellular matrices in tissues and both exhibit viscoelastic behavior. Aside from their suitable mechanical properties, hydrogels can be synthesized to be biocompatible and biodegradable and thus establish an excellent carrier for cell and tissue engineering applications.

This paper begins with an overview of the boundary value problem in the context of the elastic Eshelby inclusion problem. A few finite element simulations are included to explore the response of actual cells of non-ellipsoidal geometries. A brief review of viscoelasticity theory is followed by a characterization of the materials, both gel and cell. Then, our previous elastic inclusion analysis is leveraged to solve the corresponding viscoelastic problem by exploiting the Correspondence Principle of

---

\*Address all correspondence to this author. Email: mkazemi@umich.edu

Viscoelasticity. Taking advantage of periodic cell contractions, a Discrete Fourier Transform analysis enables fast computation of time-dependent histories of all mechanical fields. Finally, a parameter study is performed to investigate the influence of material properties and cell geometry.

## ESHELBY ANALYSIS

Of interest is the mechanical behavior of a live cardiomyocyte embedded in a viscoelastic hydrogel in response to a time-periodic stimulus that tends to contract the cell (Figure 1). Our previous mechanical analysis of Cell-In-Gel experiments [4] was based on the Eshelby inclusion problem [5], where the cell was treated as an ellipsoidal inclusion that undergoes an eigenstrain (transformation strain) while embedded in an infinite elastic matrix. The present work extends the Eshelby problem to account for viscoelasticity of the constituents. Before the viscoelastic analysis is presented, however, a brief review is provided here of the purely elastic Eshelby boundary value problem (BVP).

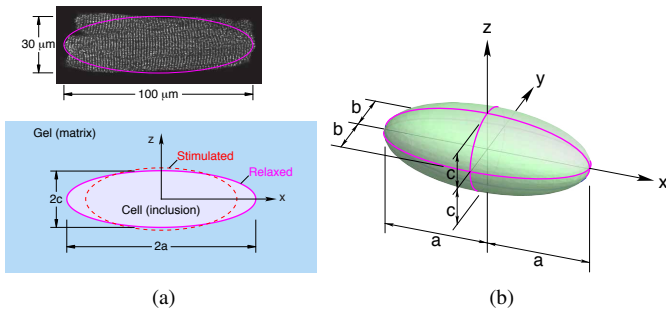


**FIGURE 1.** BOUNDARY VALUE PROBLEM ANALYZED: (A) CONFOCAL MICROGRAPH OF A CARDIOMYOCYTE AND A SCHEMATIC OF THE CELL-IN-GEL EXPERIMENT, (B) 3D SCHEMATIC OF AN ELLIPSOIDAL INCLUSION.

### Elastic Inclusion problem

When the elastic properties in the inclusion and matrix are the same, the BVP is called the *homogeneous* inclusion problem [5]. The inclusion occupies a subvolume  $V^{\mathcal{I}}$ , assumed here to have the shape of an ellipsoid (the most general shape having a known analytical solution for the BVP), and is embedded and bonded to the matrix at its periphery. The matrix, occupying the complementary volume  $V^{\mathcal{M}}$ , is assumed to be of infinite extent, so the remote boundaries are traction and displacement free. When unconstrained by the matrix, the inelastic strain in the inclusion is  $\boldsymbol{\beta}$ , called the eigenstrain (or transformation strain)<sup>1</sup>.

This simulates the load-free strain of the cell when it contracts. The presence of the matrix, however, causes the magnitude of the inclusion strain  $\boldsymbol{\varepsilon}$  to be less, since it is resisted by the surrounding matrix. This tug-of-war causes self-equilibrated (residual) stress fields inside the inclusion and within the matrix.

With respect to the Cartesian coordinate system shown in Figure 1b, the displacements  $u_i$ , strains  $\varepsilon_{ij}$ , and stresses  $\sigma_{ij}$  for the elasto-static problem are<sup>2</sup>

$$u_i(\mathbf{x}) = B_{ijk}(\mathbf{x})\beta_{jk}, \quad (1a)$$

$$\varepsilon_{ij}(\mathbf{x}) = D_{ijkl}(\mathbf{x})\beta_{kl}, \quad (1b)$$

$$\sigma_{ij}(\mathbf{x}) = C_{ijkl}[\varepsilon_{kl}(\mathbf{x}) - \Gamma(\mathbf{x})\beta_{kl}], \quad \Gamma(\mathbf{x}) = \begin{cases} 1, & \mathbf{x} \in V^{\mathcal{I}}, \\ 0, & \mathbf{x} \in V^{\mathcal{M}}, \end{cases} \quad (1c)$$

where  $\mathbf{x} = x_i\mathbf{e}_i$  is a position vector with Cartesian components  $\{x_i\} = \{x, y, z\}$  and unit base vectors  $\mathbf{e}_i$  ( $i = 1, 2, 3$ ).  $C_{ijkl}$  are the components (constants) of the 4th-order elastic stiffness tensor. The quantities  $B_{ijk}(\mathbf{x})$  and  $D_{ijkl}(\mathbf{x})$  are position-dependent components of 3rd-order and 4th-order tensors, respectively, which can be found in [5, 6].

If the elastic properties of the inclusion  $\mathbf{C}^{\mathcal{I}}$  and matrix  $\mathbf{C}^{\mathcal{M}}$  are different, the BVP is called the *inhomogeneous* inclusion problem. The problem is reduced to the previous *homogeneous* inclusion problem by introducing an equivalent eigenstrain  $\boldsymbol{\beta}^*$  that satisfies

$$C_{ijkl}^{\mathcal{I}}[S_{klmn}^0\beta_{mn}^* - \beta_{kl}] = C_{ijkl}^{\mathcal{M}}[S_{klmn}^0\beta_{mn}^* - \beta_{kl}^*], \quad (2)$$

where  $S_{klmn}^0 = D_{klmn}(\mathbf{0})$  are components of the Eshelby tensor within the inclusion (see [4]). To obtain the correct stresses and strains inside and outside the inhomogeneous inclusion, one just replaces the actual eigenstrain by the equivalent eigenstrain ( $\boldsymbol{\beta} \rightarrow \boldsymbol{\beta}^*$ ) in the previous relations for the *homogeneous* inclusion problem and proceeds by using the matrix properties  $\mathbf{C}^{\mathcal{M}}$  everywhere,

$$u_i(\mathbf{x}) = B_{ijk}(\mathbf{x})\beta_{jk}^*, \quad (3a)$$

$$\varepsilon_{ij}(\mathbf{x}) = D_{ijkl}(\mathbf{x})\beta_{kl}^*, \quad (3b)$$

$$\sigma_{ij}(\mathbf{x}) = C_{ijkl}^{\mathcal{M}}[\varepsilon_{kl}(\mathbf{x}) - \Gamma(\mathbf{x})\beta_{kl}^*]. \quad (3c)$$

For the Cell-in-Gel problem, the hydrogel (matrix) and cell (inclusion) are treated as isotropic and incompressible materials. The Young's modulus  $E$  and shear modulus  $G$  are related by  $2G = E/(1 + \nu)$  in terms of the Poisson's ratio  $\nu$ , so in the limit  $\nu \rightarrow 1/2$  the shear modulus becomes  $G = E/3$ . The dilatation

<sup>2</sup>The Einstein summation convention is assumed on repeated *lower case* latin indices within a term, as in  $x_i\mathbf{e}_i = x_1\mathbf{e}_1 + x_2\mathbf{e}_2 + x_3\mathbf{e}_3$ .

<sup>1</sup>Bold-face symbols denote vectors or higher order tensor quantities.

in this case is zero ( $\epsilon_{kk} = 0$ ), and the deformation is isochoric (volume preserving). The eigenstrain components are taken as  $\beta_{11} = \beta, \beta_{22} = \beta_{33} = -\beta/2$ , and  $\beta_{12} = \beta_{23} = \beta_{31} = 0$ , where  $\beta$  is the eigenstrain along the cell's long axis. As shown in [4] the stresses become

$$\sigma_{ij}(\mathbf{x}) = 2G^{\mathcal{M}} [\epsilon_{ij}(\mathbf{x}) - \Gamma(\mathbf{x}) \beta_{ij}^*] + p(\mathbf{x}) \delta_{ij}, \quad (4)$$

where the mean stresses in the inclusion and matrix are

$$p(\mathbf{x}) = \begin{cases} 3G^{\mathcal{M}}\beta^* \left[ \frac{I_1(0)}{4\pi} - \frac{1}{3} \right], & \mathbf{x} \in V^{\mathcal{I}} \\ 3G^{\mathcal{M}}\beta^* \left[ \frac{I_1(\lambda) - \Lambda(\lambda)x_1^2 \alpha_1^2(\lambda)}{4\pi} \right], & \mathbf{x} \in V^{\mathcal{M}} \end{cases} \quad (5)$$

where  $\beta^* = \beta_{11}^*$  and expressions for calculating  $\lambda(\mathbf{x}), \alpha_1, I_1, \Lambda$  can be found in [4]. The equivalent eigenstrains are

$$\beta_{11}^* = \frac{\beta}{P} \left[ 2\eta + \frac{\eta-1}{4\pi} (-I_2 + I_3 - 3b^2 I_{22} + 2c^2 I_{23} - 3c^2 I_{33}) \right], \quad (6a)$$

$$\beta_{22}^* = \frac{\beta}{P} \left[ -\eta + \frac{\eta-1}{4\pi} (2I_2 - 2I_3 - 3b^2 I_{22} - c^2 I_{23} + 6c^2 I_{33}) \right], \quad (6b)$$

$$\beta_{33}^* = \frac{\beta}{P} \left[ -\eta + \frac{\eta-1}{4\pi} (-I_2 + I_3 + 6b^2 I_{22} - c^2 I_{23} - 3c^2 I_{33}) \right], \quad (6c)$$

$$P = 2\eta^2 + \eta \frac{\eta-1}{\pi} (N_2 + N_3 + M_{32}) + 6 \left( \frac{\eta-1}{4\pi} \right)^2 (N_2 N_3 - M_{32}^2), \quad (6d)$$

$$\eta = G^{\mathcal{M}}/G^{\mathcal{I}}. \quad (6e)$$

The  $I, N$ , and  $M$  quantities involve elliptic integrals computed inside the inclusion as detailed in [4], and  $\beta_{12}^* = \beta_{23}^* = \beta_{31}^* = 0$ . The strains and stresses within the inclusion are uniform, depending only on the inclusion geometry and the relative stiffness of the matrix/inclusion  $\eta$ .

The results for an ellipsoidal inclusion are provided in Figures 2a and 2b, showing the axial strain and axial stress fields in the symmetry plane  $y = 0$ , which confirms that the fields are uniform inside the inclusion. The problem is also symmetric with respect to the planes  $x = 0$  and  $z = 0$ , so only the positive quadrant is shown. In this example, the inclusion dimensions are  $b = c = a/5$ , the shear moduli are  $G^{\mathcal{I}} = 8.3$  kPa and  $G^{\mathcal{M}} = 10.5$  kPa, and  $\beta = -0.17247$ . The fields in the matrix are non-uniform with a local strain and stress concentration in the matrix just outside  $x = a$ , but these decay quickly away from

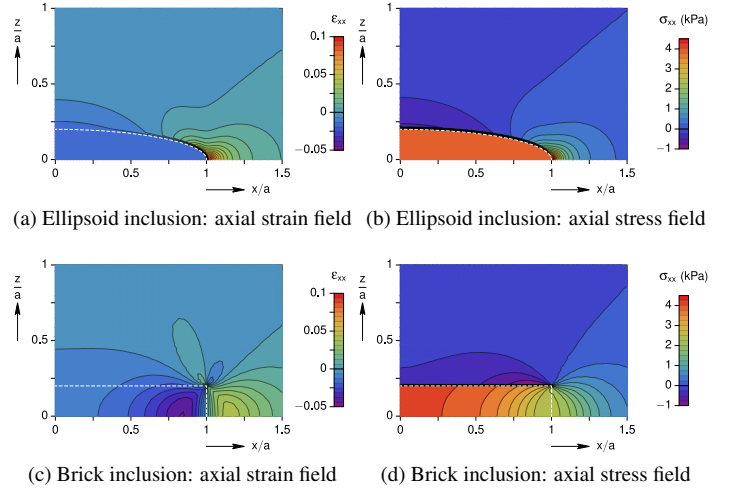


**FIGURE 2.** FINITE ELEMENT RESULTS FOR ELASTIC INCLUSIONS IN THE PLANE  $y = 0$  (POSITIVE QUADRANT)

the inclusion. The results shown in the figure were actually obtained by finite element analysis in Comsol, but they were validated with essentially perfect agreement to the Eshelby analysis calculated in Mathematica.

We also sought to determine how well an ellipsoidal inclusion represents a cardiac myocyte, which is typically more cucumber shaped. As an extreme case, the results from a second finite element simulation are shown in Figures 2c and 2d for a brick shaped inclusion with sharp corners. The aspect ratio and material properties are the same as before. As expected the strain and stress fields within the inclusion are no longer uniform, now gently varying mostly along the  $x$ -axis. The axial stress is maximum near the center of the inclusion ( $x = 0$ ) and decreases by about 20 % at the ( $x = a$ ). This is consistent with the well-known shear lag phenomena in fiber reinforced composites.

**TABLE 1.** COMPARISON OF STRESSES FOR TWO INCLUSION SHAPES

| $\sigma_{ij}$ (kPa) | Ellipsoid | Brick  |       |        |
|---------------------|-----------|--------|-------|--------|
|                     |           | Min.   | Max.  | Ave.   |
| $\sigma_{xx}$       | 3.828     | 2.122  | 4.108 | 3.654  |
| $\sigma_{yy}$       | -0.075    | -2.103 | 0.002 | -0.207 |
| $\sigma_{zz}$       | -0.075    | -2.103 | 0.002 | -0.207 |
| $\sigma_{xy}$       | 0.000     | -0.206 | 0.858 | 0.083  |
| $\sigma_{xz}$       | 0.000     | -0.206 | 0.858 | 0.083  |
| $\sigma_{yz}$       | 0.000     | -0.318 | 0.022 | -0.020 |

A summary comparison of all stress components inside the inclusion is provided in Table 1 for the two inclusion shapes. The average values are similar.

## MATERIALS

A brief review of linear viscoelasticity theory is provided below, followed by a characterization of the gel and cell materials.

### Linear Viscoelasticity

According to the theory of linear viscoelasticity, the constitutive (stress-strain) response of the material can be expressed as a convolution integral in terms of a relaxation modulus and a prescribed strain history. That is, for a given shear strain history  $\gamma(t)$ , the shear stress  $\tau(t)$  history is expressed in terms of the relaxation shear modulus  $G(t)$  as

$$\tau(t) = \int_{0^-}^t G(t-s) d\gamma(s) = G(t)\gamma(0^+) + \int_{0^+}^t G(t-s)\dot{\gamma}(s) ds, \quad (7)$$

where  $\dot{\gamma} = d\gamma/dt$  is the strain rate. If the strain input is a step function at time  $t = 0$  according

$$\gamma(t) = \begin{cases} 0, & t < 0 \\ \gamma_0, & t \geq 0 \end{cases} \quad (8)$$

where  $\gamma_0$  is a constant, the response is simply  $\tau(t) = \gamma_0 G(t)$ . Thus, the relaxation modulus  $G(t) = \tau(t)/\gamma_0$  is the stress response to a unit step strain input. For typical viscoelastic solids the stress jumps to an initial value  $G_0$  at time  $t = 0^+$  and then decays monotonically as  $t \rightarrow \infty$  to a smaller positive value  $G_\infty$ .

To capture the viscoelastic behavior of real hydrogels from rheology data with reasonable accuracy, the relaxation modulus  $G(t)$  is approximated here by a generalized Maxwell viscoelastic model. The material model consists of multiple Maxwell elements assembled in parallel, and  $G(t)$  is then mathematically represented by a Prony series according to

$$G(t) = G_\infty + \Delta G \sum_{j=1}^{N_\tau} \xi_j e^{-t/\tau_j}, \quad (9)$$

where  $\Delta G = G_0 - G_\infty$ ,  $G_\infty$  is the asymptotic value as  $t \rightarrow \infty$ ,  $\tau_j$ s ( $j = 1, 2, \dots, N_\tau$ ) are relaxation time constants (not to be confused with the shear stress), and  $\xi_j$  represent ‘phase fractions’ that apportion the amount of material that relaxes according to each time constant  $\tau_j$ . To ensure it is physically reasonable and to preserve the interpretation of  $G_0$  and  $G_\infty$  as instantaneous

and long-term values, respectively, the fractions must be non-negative  $\xi_j \geq 0$  (for all  $j = 1, 2, \dots, N_\tau$ ) and satisfy  $\sum_{j=1}^{N_\tau} \xi_j = 1$ .

If strain input is oscillatory, say  $\gamma(t) = \gamma_0 \sin \omega t$  where  $\omega$  is a prescribed angular frequency, the resulting shear stress history  $\tau(t)$  by Eq. (7) is

$$\frac{\tau(t)}{\gamma_0} = G' \sin \omega t + G'' \cos \omega t - \Delta G \sum_{j=1}^{N_\tau} \frac{\omega \tau_j \xi_j}{1 + \omega^2 \tau_j^2} e^{-t/\tau_j}, \quad (10a)$$

where

$$G' = G_\infty + \Delta G \sum_{j=1}^{N_\tau} \frac{\omega^2 \tau_j^2 \xi_j}{1 + \omega^2 \tau_j^2}, \quad (10b)$$

$$G'' = \Delta G \sum_{j=1}^{N_\tau} \frac{\omega \tau_j \xi_j}{1 + \omega^2 \tau_j^2}. \quad (10c)$$

After a sufficiently long time the decaying part can be neglected, leaving the steady oscillatory response

$$\frac{\tau(t)}{\gamma_0} = G' \sin \omega t + G'' \cos \omega t. \quad (11)$$

The quantity that characterizes the in-phase portion of the response  $G'$  is called the *storage modulus*, while that for the out-of-phase portion  $G''$  is called the *loss modulus*. These are frequency-dependent functions which can be measured in a modern dynamical mechanical analyzer. To see the phase  $\delta$  explicitly, one can rewrite Eq. (11) as  $\tau(t)/\gamma_0 = |G| \sin(\omega t + \delta)$ , where  $\tan \delta = G''/G'$  and  $|G| = \sqrt{(G')^2 + (G'')^2}$ .

Alternatively, using complex variables<sup>3</sup>, suppose the input strain history is oscillatory according to  $\hat{\gamma}(t) = \gamma_0 e^{i\omega t} = \cos \omega t + i \sin \omega t$  (by Euler’s relation) with  $i = \sqrt{-1}$  and the complex relaxation function is  $\hat{G} = G' + iG''$ . Repeating the convolution integration Eq. (7) and neglecting the decaying part, gives the response as

$$\begin{aligned} \frac{\tau(t)}{\gamma_0} &= [G' + iG''] e^{i\omega t} \\ &= [G' \cos \omega t - G'' \sin \omega t] + i [G' \sin \omega t + G'' \cos \omega t]. \end{aligned} \quad (12)$$

The real part is the response to a cosine input, and the imaginary part is the response to a sine input. Moreover, the convolution integral Eq. (7) can now be replaced by

$$\tau(t) = \hat{G}(\omega) \gamma_0 e^{i\omega t} \quad (13)$$

<sup>3</sup>denoted by a hat over a variable, such as  $\hat{\gamma}$

in terms of complex variables, when one is only interested in the limit cycle response (after transients have died out).

## Hydrogel Characterization

Rheometry measurements were performed on polyvinyl alcohol (PVA)-boronate hydrogels using a torsional dynamical mechanical analyzer with cone and plate platens. In all cases the shear strain  $\gamma$  amplitude was 2 %, and frequency scans were performed between 0.1 and 100 rad/s. Hydrogels of 10 % PVA (89-98 kDa) for several different cross-linker (CL) concentrations  $C = \{2.5, 5, 7.5, 10, 12.5, 15\}$  % were examined. Each case was run on three or four samples at 25 °C.

As an example, the results of a 10 % CL hydrogel sample are shown in Figure 3. The angular frequency was converted to cyclic frequency ( $f$  in Hz) according to  $\omega = 2\pi f$  and frequency results are shown on a logarithmic scale for clarity. In Figures 4a and 4b, the open symbols mark experimental points, and the solid black lines are fits according to Eqs. (10b) and (10c). In this case, and all others,  $G_\infty = 0$  was prescribed, since the  $G'$  was quite small at low frequencies (see the lefthand tail in Figure 4a). This means the hydrogel behaves more like a viscoelastic fluid than a viscoelastic solid.

The fits for  $G'$  and  $G''$  are reasonably good. This was achieved by selecting time constants at equal increments along a logarithmic scale,  $\tau_j = \{2^{-10}, 2^{-9}, \dots, 2^2\}$ , and then fitting with the parameters  $\xi_j$  ( $j = 1, 2, \dots, 13$ ) and  $\Delta G$ . For most of the hydrogel samples, an unconstrained fit resulted in a distribution of  $\xi$  versus  $\log \tau$  (relaxation spectrum) that resembled a Gaussian distribution. Consequently, the relaxation spectra for all of the results herein were constrained to lie along a Gaussian distribution according to

$$\xi_j = \xi(\tau_j) = \xi_0 \exp \left[ - \left( \frac{\log(\tau_j/\tau_0)}{\sigma_0} \right)^2 \right], \quad (14)$$

where  $\tau_0$  is the mean time constant,  $\sigma_0$  is the standard deviation (characteristic width) of the distribution, and  $\xi_0$  is just a normalizing constant to make  $\sum_{j=1}^{N_\tau} \xi_j = 1$ . The resulting spectrum is shown in Figure 3d. This reduced the number of fitting parameters down to only three  $\{G_0, \tau_0, \sigma_0\}$  for each hydrogel sample. The only tradeoff is that  $\tan \delta$  is somewhat over-predicted at very low frequencies (see Figure 4c).

A summary is provided in Figure 4, showing the trends of the three fitting parameters across all CL cases. The data points shown were obtained by fitting each frequency scan, similar to Figure 3. The elastic shear modulus  $G_0$  generally increases with CL concentration in a non-linear manner, although the scatter between samples becomes progressively larger. The mean time constant  $\tau_0$  also increases with CL concentration but trends almost linearly. The width of the relaxation spectrum  $\sigma_0$  is nearly constant, except at the smallest CL concentration.

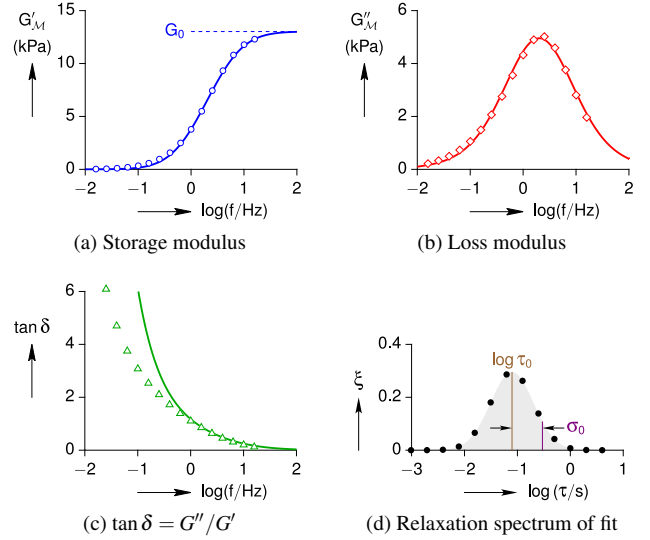


**FIGURE 3.** EXAMPLE TORSION RHEOLOGY MEASUREMENTS ON A 10 % CROSS-LINKED HYDROGEL. SOLID LINES ARE FITS USING A GAUSSIAN-LIKE RELAXATION SPECTRUM.

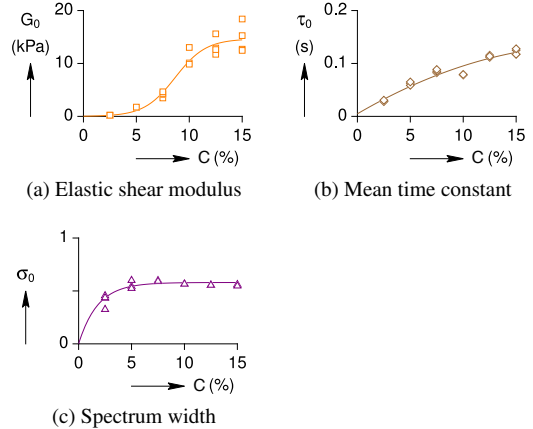


**FIGURE 4.** SUMMARY OF FITTING PARAMETERS WITH CROSS-LINK CONCENTRATION  $C$ .

The lines in Figure 4 are CL-dependent fits of the fitting parameters according to

$$G_0(C) = \frac{g_0}{2} [1 + \tanh(g_1(C - g_2))], \quad (15a)$$

$$\tau_0(C) = h_0 + h_1 C + h_2 C^2, \quad (15b)$$

$$\sigma_0(C) = s_0 [1 - e^{-s_1 C}]. \quad (15c)$$

Values of the fitting constants are provided in Table 2. This resulted in master fit functions for the complex shear moduli as a

**TABLE 2. FITTING PARAMETERS**

| $G_0$              | $\tau_0$            | $\sigma_0$   |
|--------------------|---------------------|--------------|
| $g_0 = 14.7$ (kPa) | $h_0 = 0.00486$ (s) | $s_0 = 0.58$ |
| $g_1 = 34.4$       | $h_1 = 1.17$ (s)    | $s_1 = 55$   |
| $g_2 = 0.0866$     | $h_2 = -2.62$ (s)   |              |

function of frequency and CL concentration.

### Myocyte Characterization

The elastic modulus of the cardiomyocyte was estimated using the available results from the literature. Uniaxial force-stretch measurements were performed on a single ventricular myocyte stimulated at 1.0 Hz frequency using coated micro-rods [7]. According to the extracted stress-strain response curve shown in Figure 5, the cell is assumed to be an incompressible linear elastic material with an approximate Young's modulus of  $E^{\mathcal{I}} \approx 25$  kPa.

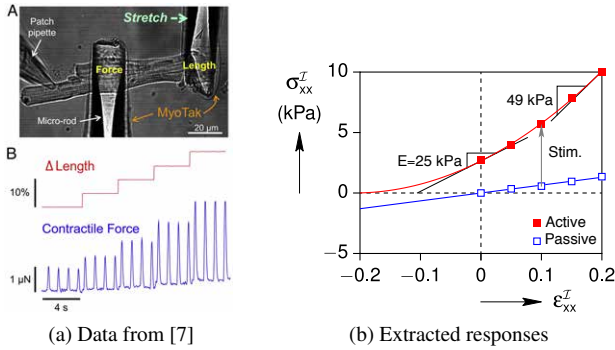


**FIGURE 5. SINGLE CELL UNIAXIAL RESPONSE**

### VISCOELASTIC ESHELBY ANALYSIS

Now we wish to account for the viscosity of the cell and gel in the framework of the Eshelby inclusion analysis. This causes all mechanical field quantities to become dependent on time  $t$ .

According to correspondence principle of linear viscoelasticity [8], if the linear elastic solution is known for a body that undergoes quasi-static motion, the solution to the corresponding problem in linear viscoelasticity can be constructed by substituting constitutive parameters with their time-dependent counterparts. The correspondence principle takes advantage of time-space separability by solving the time-dependent portion of the problem in the Laplace or Fourier domain. The principle however, is restricted to problems where the boundary conditions

(surface tractions or displacements) do not change type over time, although the surface tractions or displacements may be time-dependent. That is, for every point on the surface, either tractions are specified for all time or the displacements are specified for all time.

Taking the Fourier transform of the field equations in Eq. (3b), the pseudo-elastic solution is solved in the frequency domain by

$$\hat{u}_i(\mathbf{x}, \omega) = \hat{B}_{ijk}(\mathbf{x}, \omega) \hat{\beta}_{jk}^*(\omega), \quad (16a)$$

$$\hat{\epsilon}_{ij}(\mathbf{x}, \omega) = \hat{D}_{ijkl}(\mathbf{x}, \omega) \hat{\beta}_{kl}^*(\omega), \quad (16b)$$

$$\hat{\sigma}_{ij}(\mathbf{x}, \omega) = 2\hat{G}^{\mathcal{M}}(\omega) \left[ \hat{\epsilon}_{ij}(\mathbf{x}, \omega) - \Gamma(\mathbf{x}) \hat{\beta}_{ij}^*(\omega) \right] + \hat{p}(\mathbf{x}, \omega) \delta_{ij}. \quad (16c)$$

An arbitrary eigenstrain history can be expressed as the Complex Fourier Series

$$\beta(t) = \sum_{n=-\infty}^{\infty} \hat{\beta}_n e^{i\omega_n t}, \quad (17)$$

where the coefficients are complex valued  $\hat{\beta}_n = \beta'_n + i\beta''_n$ . Since  $\beta(t)$  are real valued, the coefficients  $\hat{\beta}_n$  and  $\hat{\beta}_{-n}$  are complex conjugates. The stress response to Eq. (17) is just the superposition of responses at each individual frequency, since the viscoelastic constitutive relations are linear. Thus, the generalization of Eq. (16c) is the stress tensor (suppressing the spatial arguments)

$$\boldsymbol{\sigma}(t) = \sum_{n=-\infty}^{\infty} 2\hat{G}_n^{\mathcal{M}} \left[ \hat{\boldsymbol{\epsilon}}_n - \Gamma \hat{\boldsymbol{\beta}}_n^* \right] + \hat{p}_n \boldsymbol{\delta}, \quad (18)$$

where  $\hat{G}_n = \hat{G}(\omega_n)$  are the complex relaxation moduli at each frequency. This relation provides the steady state oscillatory response to a periodic eigenstrain input. The coefficients  $\hat{\beta}_n$  are found in the usual way by multiplying Eq. (17) through by  $e^{-i\omega_m t}$  with  $\omega_m = 2\pi m/T$ , integrating across the interval  $t \in [-T/2, T/2]$ , and exploiting orthogonality of integrals involving  $\exp(i2\pi(n-m)t/T)$ , resulting in

$$\hat{\beta}_n = \frac{1}{T} \int_{-T/2}^{T/2} \beta(t) e^{-i2\pi n t/T} dt. \quad (19)$$

If the eigenstrain input is measured at  $N$  equal time increments ( $\Delta t = T/N$ ) within a periodic cycle, the sequence is

$$\beta_m = \beta(m\Delta t), \quad \text{for integers } m = -\frac{N}{2}, \dots, \frac{N}{2} - 1. \quad (20)$$

which assumes  $N$  is even<sup>4</sup>. This leads to the Discrete Fourier Transform (DFT), where Eq. (19) is approximated by

$$\widehat{\beta}_n \approx \frac{1}{N} \sum_{m=-N/2}^{N/2-1} \beta_m e^{-i2\pi nm/N}, \quad n = -\frac{N}{2}, \dots, \frac{N}{2} - 1, \quad (21)$$

and the inverse DFT, replacing Eq. (17), is

$$\beta_m = \sum_{n=-N/2}^{N/2-1} \widehat{\beta}_n e^{i2\pi nm/N}. \quad (22)$$

Finally, using Eq. (18) the stress response at discrete times becomes

$$\sigma_m = \sigma(m\Delta t) = \sum_{n=-N/2}^{N/2-1} 2G_n^M \left[ \widehat{\epsilon}_n - \Gamma \widehat{\beta}_n^* \right] + \widehat{p}_n \delta. \quad (23)$$

Note that one needs to be careful about the ordering of frequencies to ensure the complex modulus is summed over complex conjugate pairs with respect to real frequencies. That is, when using Eq. (10) with  $\omega_n = 2\pi n/T$ , we need  $G'(\omega_n) = G'(-\omega_n)$  and  $G''(\omega_n) = -G''(-\omega_n)$ . This is why we prefer the quasi-symmetric summation about  $n = 0$  (rather than  $n = 1, \dots, N$  or  $n = 0, \dots, N-1$  that is often used).

## VE Eshelby Simulations

In this Section, the viscoelastic Eshelby model is used to calculate the multi-axial stress and strain time responses of an ellipsoidal cell inside a typical gel. A baseline case is first presented, and the simulated axial strain history is compared to the results of a Cell-in-Gel experiment. A parametric study is then carried out to investigate the influence of geometric and material properties of the system on the stress and strain time responses.

### Baseline Study

As a baseline case, the multi-axial steady-oscillation time histories are studied for an elastic inclusion (cell) of  $G_0^I = 8.3$  kPa inside a viscoelastic matrix (hydrogel) with a crosslink density of  $C = 10\%$ . Consistent with the actual cardiomyocyte in the Cell-in-Gel experiment, the ellipsoidal cell is considered to have an aspect ratio of  $a/b = 5$  with  $c = b$ . The experiment recorded the axial strain history of a cardiomyocyte electrically stimulated at about 0.5 Hz after many cycles while embedded in the gel (shown by black line in Figure 6a). The maximum contraction was about  $-11\%$  strain. The cross-linker was then dissolved

away (leaving a nearly inviscid water/PVA fluid) and the strain history of the same myocyte was measured under nearly load-free conditions (shown by gray line in Figure 6a). As expected, the maximum contraction in this case was larger, about  $-17\%$  strain. This load-free strain history was used as the eigenstrain input to the viscoelastic Eshelby analysis.

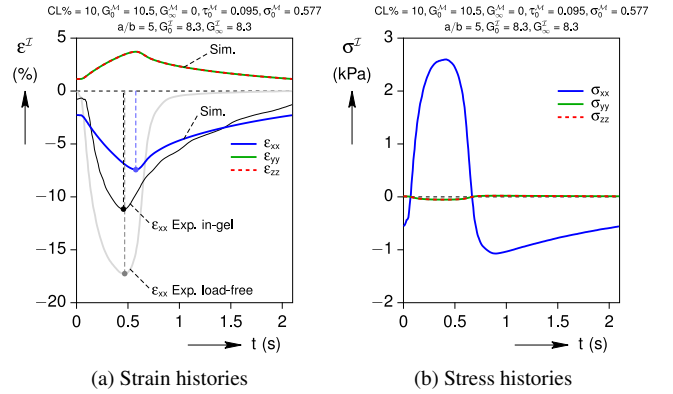


**FIGURE 6.** MULTIAXIAL STRAIN AND STRESS TIME RESPONSES IN THE INCLUSION FOR THE BASELINE CASE

The predicted axial strain history  $\epsilon_{xx}$  (as shown by the blue line in Figure 6a) has the right qualitative character, but the peak contraction (about  $-7\%$  strain) is less than the measured experimental value. This is due to the fact that the actual myocyte significantly up-regulates its internal  $\text{Ca}^{2+}$  transients (measured, but not shown here) that increase contractility in response to the resistance provided by the hydrogel. This is the cellular origin of the Anrep effect in the whole heart in response to increased afterload. This adaptive feature is not captured here in the Eshelby model. Also, as expected for a contractile, but otherwise passive, inclusion there is a 5% time-lag between the simulated strain peak and the load-free eigenstrain; whereas, no time lag is detectable in the measured axial strain in-gel. It can also be seen from Figure 6b that the predicted peak stresses precede maximum contraction, due to the viscosity of the gel. The stress state in the inclusion is multi-axial, but the shear stresses are zero and the lateral stresses are quite small due to the slenderness of the ellipsoid.

### Parametric Study

Numerous simulations have been performed to understand parametric sensitivities of the Cell-in-Gel system with respect to the stiffness and aspect ratio of the cell, and the viscoelastic properties of the gel. As demonstrated in Figure 7a, the gel cross-link concentration,  $C$  has a strong effect on the cell contraction such that the predicted magnitude of strain inside the

<sup>4</sup>If  $N$  is odd,  $m = -\frac{N-1}{2}, \dots, \frac{N-1}{2}$

cell is significantly reduced and the phase difference between the stimulus signal and the contraction response is increased as the crosslink density is enhanced. Similarly, the magnitude of predicted stresses are increased and the residual stress recovery is delayed with increased crosslink density of hydrogel.

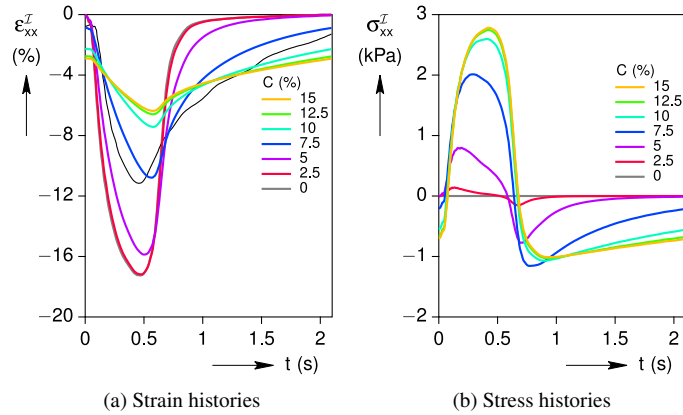


**FIGURE 7.** EFFECT OF GEL CROSS-LINK CONCENTRATION ON THE AXIAL STRAIN AND STRESS TIME HISTORIES IN THE INCLUSION

In another study, the influence of cell aspect ratio,  $a/b$ , has been investigated. It can be seen from Figure 8, that changing aspect ratio has a moderate effect on time histories of stress and strain curves such that somewhat larger stress and reduced contraction is observed for slender cells (higher  $a/b$ ). This is due to the fact that for a fixed value of  $b$  (and  $c$ ), increasing the aspect ratio would increase the total surface of the cell that is in contact with the gel and subsequently the cell would experience higher stresses against contraction (inside the gel), for the same stimulus.

To better understand the effect of up-regulation on the time response of the system, the effect of cell stiffness,  $G_0^I$ , has been considered on stress and strain curves. This is an important study since cardiac myocytes are well known to up-regulate their  $Ca^{2+}$  transients in response to afterload (Anrep effect). As presented in Figure 9a, the cell elastic stiffness has a large effect, and the agreement with measurement of peak contraction at augmented values indicates one possible manifestation of up-regulation.

## CONCLUSIONS

Here we provide a 3-D mechanical analysis of a single myocyte beating in a viscoelastic hydrogel that mimics the *in vivo* mechanical environment in myocardium under certain pathological conditions. As a necessary step towards understanding the

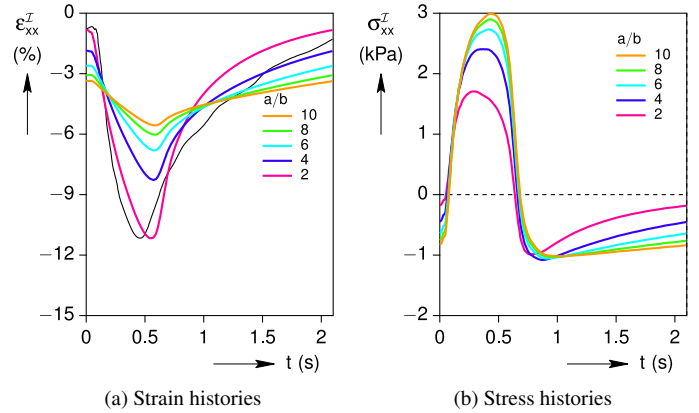


**FIGURE 8.** EFFECT OF CELL ASPECT RATIO ON THE AXIAL STRAIN AND STRESS TIME RESPONSES IN THE INCLUSION

mechanical stress effects on the heart function and disease development, we present a general analytic solution for inhomogeneous viscoelastic Eshelby inclusion problem that facilitates parametric studies of the *in vitro* cell-in-gel experiment and provides a quantitative mapping of the mechanical strain and stress inside and outside the myocyte. Our analyses reveal that the change in myocyte stiffness, as a result of the up-regulation of the  $Ca^{2+}$  transients, has a strong influence on the contraction of the cell in response to the afterload. The findings also demonstrate that increasing hydrogel's crosslink density, in the cell-in-gel experiment, will significantly alter the strain and stress fields inside the cell and yields to an increased time-lag in the response of the myocyte to the external stimulus. The results of the present

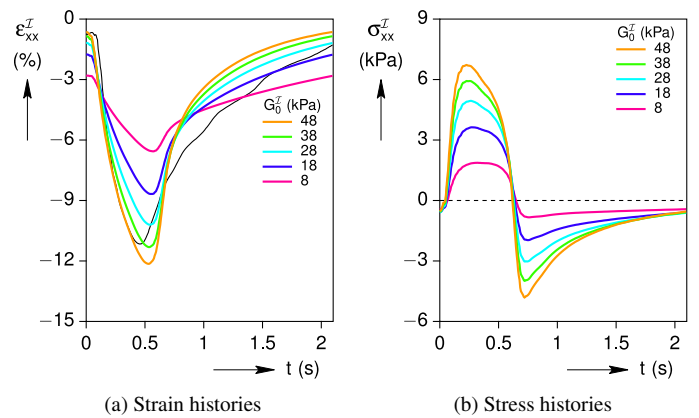


**FIGURE 9.** UP-REGULATION EFFECT ON THE STRESS AND STRAIN TIME RESPONSE CURVES

model is in good agreement with the experimental contraction measurements of the cell-in-gel experiment and will inform studies of the mechanotransduction mechanisms that link mechanical stress to cardiac function and remodeling in health and disease.

## REFERENCES

- [1] von Anrep, G., 1912, "On the part played by the suprarenals in the normal vascular reactions of the body," *The Journal of physiology*, 45(5), pp. 307–317.
- [2] Bollensdorff, C., Lookin, O., and Kohl, P., 2011, "Assessment of contractility in intact ventricular cardiomyocytes using the dimensionless 'Frank-Starling Gain' index," *Pflügers Archiv : European Journal of Physiology*, 462(1), p. 39.
- [3] Jian, Z., Han, H., Zhang, T., Puglisi, J., Izu, L. T., Shaw, J. A., Onofriok, E., Erickson, J. R., Chen, Y.-J., Horvath, B., Shimkunas, R., Pan, T., Chan, J., Banyasz, T., Chiamvimonvat, N., Bers, D. M., Lam, K. S., and Chen-Izu, Y., 2014, "Mechanochemotransduction During Cardiac Contraction Is Mediated by Localized Nitric Oxide Signaling," *Science Signaling*, 7(317), pp. 1–9.
- [4] Shaw, J. A., Izu, L. T., and Chen-Izu, Y., 2013, "Mechanical Analysis of Single Myocyte Contraction in a 3-D Elastic Matrix," *PLOS ONE*, 8(10), p. e75,492.
- [5] Eshelby, J. D., 1957, "The determination of the elastic field of an ellipsoidal inclusion, and related problems," *Proc Royal Soc A*, 241(1226), pp. 376–396.
- [6] Eshelby, J. D., 1959, "The Elastic Field Outside an Ellipsoidal Inclusion," *Proc. Roy. Soc. London. Series A, Math. & Phys. Sci.*, 252(1271), pp. 561–569.
- [7] Prosser, B. L., Khairallah, R. J., Ziman, A. P., Ward, C. W., and Lederer, W. J., 2013, "X-ROS signaling in the heart and skeletal muscle: Stretch-dependent local ROS regulates  $[Ca^{2+}]_i$ ," *Journal of Molecular and Cellular Cardiology*, 58, p. 172.
- [8] Wineman, A. S. and Rajagopal, K. R., 2000, *Mechanical Response of Polymers*, Cambridge University Press.